On limb radiance calculations and convergence of relaxation type retrieval algorithms

L. Rezac,[1,*] A. A. Kutepov,[2,3] A. G. Feofilov,[2,3] and J. M. Russell, III[1]

[1]Center for Atmospheric Sciences, Hampton University, 23 Tyler Street, Hampton, Virginia 23668, USA

[2]NASA Goddard Space Flight Center, Greenbelt, Maryland, USA

[3]The Catholic University of America, Washington, District of Columbia, USA

*Corresponding author: ladislav.rezac@hamptonu.edu

Received 15 February 2011; revised 27 May 2011; accepted 19 August 2011;
posted 24 August 2011 (Doc. ID 142603); published 30 September 2011

Several approaches to the solution of the radiative transfer equation assume either Curtis–Godson average or linear change of the source function across grid segments. When such solutions are used for calculating limb radiances, the peak radiance response to the source function perturbation at tangent point i is displaced down to the tangent point $i+1$. This effect is explained through a geometric argument. Temperature profile retrievals performed by applying the ratio of signals at level $i+1$ for correcting temperature at level i demonstrate dramatic convergence acceleration of the iterative relaxation scheme. © 2011 Optical Society of America

OCIS codes: 010.0280, 260.3090, 280.4991, 280.6780.

1. Introduction

The principles of limb scanning instruments observing thermal emissions from the atmosphere have been thoroughly described by early investigators of this technique, see [1,2]. The advantages of scanning the planetary limb stem directly from the geometry of the observations and the exponential decrease of density with height. The energy emitted from the atmosphere is recorded against the cold background of space, eliminating a need for removal of a background radiation. The vertical resolution for limb observations is determined by spatial weighting functions (as opposed to purely spectral weighting functions for nadir instruments) that are usually peaked at the tangent layers. In addition, the limb geometry ensures for an infinitesimal field-of-view (FOV) that no contribution to the measured radiances comes from altitudes just below the tangent height.

In the study presented here, we investigated the response of synthetic broadband 15 μm CO_2 limb radiances in the Earth's atmosphere to the perturbation of the source function caused by kinetic temperature perturbations. The study was performed during retrieval algorithm analysis of the sounding of the atmosphere using broadband emission radiometry (SABER) instrument on board the thermosphere ionosphere mesosphere energetics and dynamics (TIMED) satellite (see [3] for the instrument description and [4] for an overview of 15 μm emissions used for the temperature retrievals). Hereforth the 15 μm emissions will be referred to as SABER Ch1 (channel 1) emissions.

The accelerated lambda iteration for atmospheric radiation and molecular spectra (ALI-ARMS) [5–7] code package was used for calculating vibrational level populations with accounting for the departure from local thermodynamic equilibrium (non-LTE). The limb radiance calculations were performed on a 1 km vertical grid with the assumption of an infinitesimal FOV function.

We demonstrate that modeling the limb radiances with an interpolation or Curtis–Godson averaging of the source function across grid segments leads to a downward displacement of the 15 μm peak radiance

0003-6935/11/285499-04$15.00/0

response to the source function perturbation. That is, the largest change in limb radiance is at level $i+1$ (one grid point below i), in response to the source function perturbation at tangent height i. A simple geometric argument is presented for the explanation of this effect.

The sample calculations shown in this paper use climatological equatorial daytime atmosphere. The altitude range of the synthetic retrievals extends from 65 to 120 km. The forward modeling investigations of the limb radiance response to the temperature perturbations were performed for the altitude region 40–120 km and demonstrated the presence of the above described response displacement all over this region for a number of atmospheric models studied.

Finally, we show that, accounting for the sensitivity shift yields a significant improvement in the convergence rate of the temperature relaxation retrieval algorithm and discuss general implications of our results for other relaxation retrieval schemes.

2. Radiance Sensitivity Displacement

The expression for simulating radiances for a limb viewing experiment with an infinitesimal FOV can be written as

$$I(\nu,h)=\int_{\nu}\mathrm{d}\nu\quad\phi(\nu)\int_{x}\mathrm{d}x\quad S(\nu,x)\frac{dt(\nu,x)}{dx},\qquad(1)$$

where the integral represents the formal solution of the radiative transfer equation (RTE) evaluated along the line-of-sight (LOS) for a particular ray intersecting a tangent layer h. $S(\nu,x)$ is the source function, $t(\nu,x)$ is the transmittance from point x to the observer, and $\phi(\nu)$ is the instrumental spectral response function. The usual assumption of spherical symmetry of the atmosphere is made when calculating the limb radiances.

Several methods of RTE solution implemented in ALI-ARMS code [6] were utilized during this study. Among them are the long and short characteristics of the zero- and first-order [8], which work with the integral form of the RTE, the Feautrier [9], and the discontinuous finite elements method (DFE) [10] that solve the RTE in the form of a difference equation. Long and short characteristics of the zeroth order utilize the source function presented as a step-function with value for each segment defined in various ways: (a) as that at one of the segment boundaries, (b) as mean of its values at segment boundaries, or (c) as Curtis–Godson average along the segment, whereas those of first-order based on the linear change of the source function within each pass segment. On the other hand, both DFE and Feautrier methods implicitly utilize linear interpolation of source function within each segment. We mention here, that there are also numerous methods of varying sophistication in existence, in addition to those tested here, however, in this study we did not go beyond the linear interpolation of the source function along the LOS which was proved to be both most stable and sufficiently accurate. It avoids occasional unwanted oscillations that higher-order interpolation schemes are prone to develop [8,11].

During our study of the temperature retrieval algorithm applied to the SABER Ch1 radiances, we analyzed the ratios of simulated limb radiances obtained when the kinetic temperature profile T_k was perturbed by some amount ΔT_k at a certain tangent height (I_{new}) to those obtained for unperturbed sets of atmospheric parameters (I_{orig}). In Fig. 1, these ratios are displayed for the case of a $\Delta T_k=+2$ K change applied at the tangent height level i of 100 km. The solid curve in Fig. 1(a) was obtained when the DFE algorithm, which utilizes linearly varying source function across the grid segments, was applied for calculating limb radiances. It illustrates the downward vertical displacement of the peak radiance response to the temperature perturbation: perturbing T_k at tangent point, i, results in the largest response in the calculated radiance occurring at the tangent height of one vertical grid point below, i.e., at $i+1$. The dashed curve in Fig. 1(a) corresponds to the same perturbation conditions; however, radiances were obtained by means of the long-characteristics algorithm with the source function presented as a step-function with the value for each pass segment equal to the value at the lower boundary of the corresponding spherical shell (see Fig. 2 below). It demonstrates no displacement of radiance response. It should also be noted the two curves in Fig. 1(a) exhibit the well-known downward broadening of the radiance response caused by the limb weighting functions. The latter are shown in Fig. 1(b) for tangent heights 97, 98, 99, and 100 km.

Figure 2 illustrates a geometric argument how the downward displacement comes about when the source function is interpolated across the segments. Let the source function S_2 at the tangent grid point 2 for ray 1 experience a perturbation. Because of the

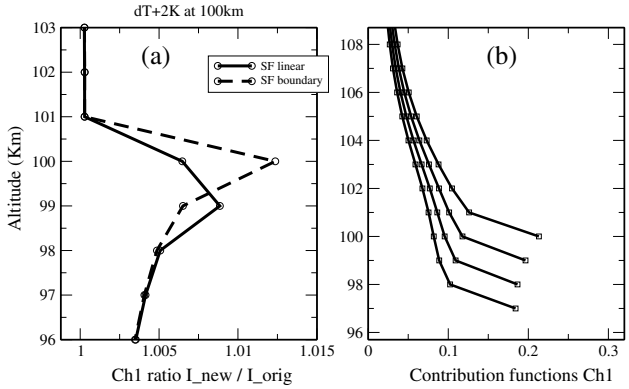

Fig. 1. (a) Vertical displacement of the peak radiance response to the T perturbation using a linear interpolation of the source function (solid curve). The dashed curve illustrates that no displacement takes place when the source function is presented as a step-function with a constant value for each shell equal to the value at the lower boundary. (b) Four Ch1 limb contribution functions for tangent heights 97, 98, 99, and 100 km.

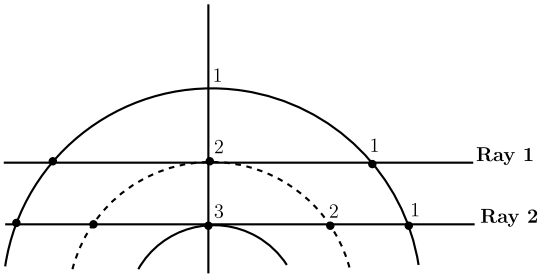

Fig. 2. Illustration of the geometrical argument. The strongest radiance sensitivity to the change of ΔT_k at tangent layer, i, is experienced at tangent layer $i+1$. The numbers indicate the grid boundaries at which the source function and other atmospheric parameters are prescribed. See text for description.

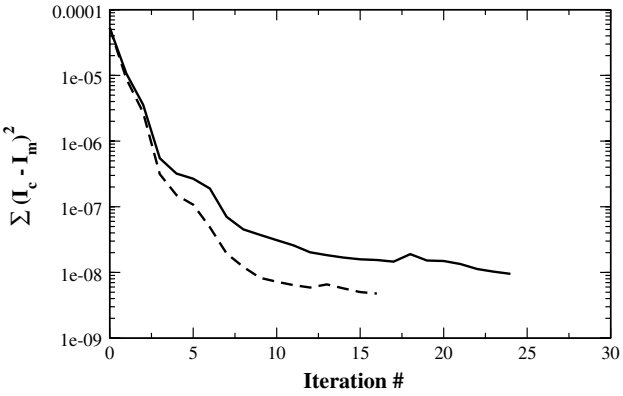

Fig. 3. Convergence curves for the T_k retrieval. The number of iterations is on the horizontal axis and the sum of squared differences between calculated, I_c, and measured, I_m, radiances is on the vertical axis. The sum is taken over the entire retrieval altitude range of 65–120 km. See text for discussion.

spherical symmetry assumption, this change will implicitly occur over the entire spherical surface 2. This is depicted by the dashed arc in the Fig. 2.

Because of the interpolation applied, this perturbation impacts both spherical shells 1–2 and 2–3. Since the sum of the geometrical lengths affected by the source function increases for ray 2 compared to ray 1 (by about 40%) and the pressure increases exponentially with decreasing altitude, the peak of radiance sensitivity in response to the source function perturbation at grid point 2 shifts down from ray 1 to ray 2.

It follows from the geometrical analysis presented above that it should be of little consequence what order of interpolation is used across the segments, be it piecewise (such that the segment source function $S_{i,i=1} = 0.5 \times (S_i + S_{i+1})$), linear, or even higher-order. RTE solving algorithms using a linear interpolation or a piecewise linear interpolation were tested in this study and all of them demonstrated the downward sensitivity displacement. The same is also true when Curtis–Godson averaging was applied across pass segments.

3. Displaced Radiance Sensitivity Impact on the T_k Retrieval

The significance of the altitude peak radiance response shift is realized when interpreted as a down shift of information about ΔT_k change from a level i to a new level $i+1$. This shift should be taken into account for temperatures updating in any relaxation type algorithm, be it a sequential type, such as "onion peeling" [12] or a global fit [13], which updates parameters at all altitudes simultaneously.

In Fig. 3 the effect of accounting for the down shift of the radiance sensitivity is demonstrated for the case of temperature retrieval from the Ch1 noiseless radiance starting with an initial guess shifted by −15 K from the temperature profile used for simulating the measured signal. The temperature correction scheme used is similar to that of [14] applied for T_k retrievals from the cryogenic infrared spectrometers and telescopes for the atmosphere (CRISTA) instrument. The limb radiance calculations were performed with DFE algorithm.

The solid black line shows convergence rate for the standard correction scheme, i.e. updating T_k at tangent height, i from radiance ratio at the height i. The dashed curve represents the convergence rate when the correction function uses the ratio of radiances at the $i+1$ level to update T_k at level i. One may see in this figure that making corrections at level i by applying the ratio of signals at level $i+1$ causes dramatic reduction of the number of iterations for the same signal fitting compared to the standard correction scheme: the number of iterations required to reach the convergence criteria $10e-8$ is reduced by a factor of about 3 (8 iterations against 23 iterations). The observed acceleration of convergence is not unique to the tropical atmospheric model, but is ubiquitous for large variety of atmospheric conditions tested. Similar convergence acceleration was observed when DFE algorithm on limb was replaced by Feautrier one and by the long-characteristics with the stepwise function $S_{i,i=1} = 0.5 \times (S_i + S_{i+1})$ and with that estimated as Curtis–Godson average along each pass segment. We also note here that, in all these tests the retrieval accuracy was not significantly affected by taking into account the radiance sensitivity displacement.

In general, it should be realized that an iterative relaxation retrieval for temperature from the limb radiances is a complex nonlinear problem. The retrieval performance depends on many factors such as the correction scheme applied, how far the initial guess is from the true profile, nonlinearity, etc. Changing these factors may increase the importance of taking into account the displaced sensitivity or it may render it less important. For example, in our tests when the algorithm converged within five iterations (usually in case of initial temperature guess taken to be close to true profile), we observed little or no effect of convergence improvement when accounting for the displaced sensitivity. Nevertheless, from a theoretical perspective, it is a goal to utilize in a best way all information available for temperature correction during the iterative retrieval, and,

therefore, accounting for the displaced sensitivity is desirable.

4. Conclusion

A downward displacement of the peak radiance response to the source function perturbation is observed in our modeling of the 15 μm limb radiances for the SABER/TIMED instrument. This displacement is a result of the linear interpolation of the source function across the LOS path segments in combination with the limb geometry and homogeneous spherical shells assumption. It is also reasonable to suppose that a higher-order interpolation scheme for the source function will exhibit a similar effect. We also show that accounting for this displacement in the relaxation retrieval algorithm applied for temperature retrievals from the SABER broadband 15 μm limb radiances leads to a dramatic increase of the algorithm convergence rate. This is the result of better information utilization from the limb radiances when the correction function accounts for the displaced sensitivity. On the other hand, no significant improvement in temperature retrieval accuracy or radiance fitting is achieved over an algorithm that uses information directly at level, i. However, this algorithm requires about three times more iterations to achieve the same radiance fitting for the given initial conditions.

The study presented was performed for an infinitesimal FOV function aimed at applications to the SABER observational data processed with applying FOV deconvolution. However, additional numerical tests were made modeling the limb radiance with a finite square FOV function of varying vertical extend. These calculations demonstrate the vertical displacement of radiance sensitivity from tangent height h to the tangent height $h + 0.5 \times \gamma$, where γ is the full-width-half-maximum (FWHM) of the square FOV function at the vertical axes.

Finally, it is worth noting that the downward sensitivity shift in response to the source function perturbation will be observed for limb radiances calculated with any interpolation scheme, be it linear, stepwise linear, or Curtis–Godson averaging of the source function regardless of LTE versus non-LTE, atmospheric composition, spectral region, etc. The question whether source function is responsive to the perturbation of specific atmospheric parameter is of secondary importance for the understanding of the effect discussed in this paper, even though it is important from a practical point of view. Obviously, accounting for the sensitivity displacement may improve a relaxation type retrieval algorithm performance only if the perturbation of the parameter to be retrieved has significant impact on the source function. This is true for a temperature perturbation in the case of local thermodynamic equilibrium (LTE) when the source functions coincide with the Planck functions. It also worked perfectly in our case of temperature retrievals from the SABER 15 μm limb radiances for the Earth's mesosphere and lower thermosphere. In this altitude region the departure from LTE for CO_2 transitions in the 15 μm spectral region is moderate [15] and, therefore, source functions remain sensitive to the temperature perturbations.

References

1. J. C. Gille and F. B. House, "On the inversion of limb radiance measurements 1: temperature and thickness," J. Atmos. Sci. **28**, 1427–1442 (1971).
2. J. C. Gille and P. L. Bailey, "Inversion of infrared limb emission measurements for temperature and trace gas concentrations," in *International Interactive Workshop on Inversion Methods in Atmospheric Remote Sensing*, (Academic, 1977) pp. 195–216.
3. J. M. Russell III, M. G. Mlynczak, L. L. Gordley, J. Tansock, and R. Esplin, "An overview of the SABER experiment and preliminary calibration results," Proc. SPIE Int. Soc. Opt. Eng. **3756**, 277–288 (1999).
4. C. J. Mertens, M. G. Mlynczak, M. López-Puertas, P. P. Wintersteiner, R. H. Picard, J. R. Winick, L. L. Gordley, and J. M. Russell III, "Retrieval of mesospheric and lower thermospheric kinetic temperature from measurements of CO_2 15 μm Earth limb emission under non-LTE conditions," Geophys. Res. Lett. **28**, 1391–1394 (2001).
5. A. A. Kutepov, O. A. Gusev, and V. P Ogibalov, "Solution of the non-LTE problem for molecular gas in planetary atmospheres: Superiority of accelerated lambda iteration," J. Quant. Spectrosc. Radiat. Transfer **60**, 199–220 (1998).
6. O. A. Gusev and A. A. Kutepov, "Non-LTE gas in planetary atmospheres," in *Stellar Atmosphere Modeling*, I. Hubeny, D. Mihalas, and K. Werner, eds., Vol. 288 in ASP Conference Series (ASP, 2003), pp. 318–331.
7. O. Gusev, "Non-LTE diagnostics of the infrared observations of the planetary atmosphere," Ph. D. thesis (Ludwig-Maximilians University, Munchen, 2002).
8. G. L. Olson and B. P. Kunasz, "Short characteristic solution of the non-LTE line transfer problem by operator perturbation I. The one dimensional planar slab," J. Quant. Spectrosc. Radiat. Transfer **39**, 325–336 (1987).
9. D. Mihalas, *Stellar Atmospheres* (Freeman, 1978).
10. J. I. Castor, P. G. Dykema, and R. I. Klein, "A new scheme for multidimensional line transfer. II—ETLA method in one dimension with application to iron K-alpha lines," Astrophys. J. **387**, 561–571 (1992).
11. E. Griffioen and L. Oikarinen, "LIMBTRAN: A pseudo three-dimensional radiative transfer model for the limb viewing imager OSIRIS on the ODIN satellite," J. Geophys. Res. **105**, 29717–29730 (2000).
12. J. M. Russell III and S. R. Drayson, "The inference of atmospheric ozone using satellite horizon measurements in the 1042 cm^{-1} band," J. Atmos. Sci. **29**, –(1971).
13. M. Carlotti, "Global-fit approach to the analysis of limb-scanning atmospheric measurements," Appl. Opt. **27**, 3250–3254 (1988).
14. O. A. Gusev, M. Kaufmann, K.-U. Grossmann, F. J. Schmidlin, and M. G. Shepherd, "Atmospheric neutral temperature distribution at the mesopause altitude," J. Atmos. Sol. Terr. Phys. **68**, 1684–1697 (2006).
15. M. López-Puertas and F. W. Taylor, *Non-LTE Radiative Transfer in the Atmosphere* (World Scientific, 2001).